

# Computing band gaps of periodic materials via sample-based quantum diagonalization

Alan Duriez<sup>1,7†</sup>, Pamela C. Carvalho<sup>2,9†</sup>,  
Marco Antonio Barroca<sup>1,8†</sup>, Federico Zipoli<sup>3,10</sup>, Ben Jaderberg<sup>4</sup>,  
Rodrigo Neumann Barros Ferreira<sup>1</sup>, Kunal Sharma<sup>5</sup>,  
Antonio Mezzacapo<sup>5</sup>, Benjamin Wunsch<sup>6</sup>, Mathias Steiner<sup>1\*</sup>

<sup>1</sup>IBM Research, Rio de Janeiro, 20031-170, RJ, Brazil.

<sup>2</sup>IBM Research, São Paulo, 04007-900, SP, Brazil.

<sup>3</sup>IBM Research Europe, Zurich, 8803, Rüschlikon, Switzerland.

<sup>4</sup>IBM Research Europe, Hursley, Winchester, SO21 2JN, United Kingdom.

<sup>5</sup>IBM Quantum, IBM T.J. Watson Research Center, Yorktown Heights, New York, 10598, NY, USA.

<sup>6</sup>IBM Research, IBM T.J. Watson Research Center, Yorktown Heights, New York, 10598, NY, USA.

<sup>7</sup>Instituto de Física, Universidade Federal Fluminense, Niterói, 24210-346, RJ, Brazil.

<sup>8</sup>Centro Brasileiro de Pesquisas Físicas, Rio de Janeiro, 22290-180, RJ, Brazil.

<sup>9</sup>Instituto de Física da Universidade de São Paulo, Universidade de São Paulo, São Paulo, 05508-090, SP, Brazil.

<sup>10</sup>National Center for Competence in Research-Catalysis (NCCR-Catalysis), Zurich, Switzerland.

\*Corresponding author(s). E-mail(s): [mathiast@br.ibm.com](mailto:mathiast@br.ibm.com);

Contributing authors: [alanduriez@ibm.com](mailto:alanduriez@ibm.com);

†These authors contributed equally to this work.

## Abstract

State-of-the-art techniques in computational materials science often fail to capture many-body interactions in periodic systems. One particular application is the electronic structure problem, where established approaches such as Density

Functional Theory are applied to predict experimental results. In this contribution, we present a sample-based quantum diagonalization (SQD) workflow for simulating the electronic ground state of periodic materials, and for predicting their band gaps. We obtain a fermionic Hamiltonian for crystalline solids by first projecting the electronic density obtained by density functional theory onto a localized basis set and then adding interaction parameters obtained by a self-consistent field theory. We then build an approximation of the system's ground-state wavefunction with the local unitary cluster Jastrow (LUCJ) ansatz. By sampling the quantum circuit and classically diagonalizing the Hamiltonian in the resulting configuration subspace, we predict the band gap energy of representative materials and obtain agreement with experimental results. The predicted bandgaps were obtained from calculations using 38 and 46 qubits, performed on a superconducting quantum processor, with minimal error-mitigation overhead. Our self-consistent approach offers a scalable pathway for utility-scale quantum simulation of materials.

**Keywords:** material science, quantum computing, quantum simulation

A considerable effort in the fields of materials science and computational chemistry is devoted to building simulation algorithms for predicting material properties [1]. This enables the analysis of materials while eliminating the need for costly experimental methods. One of the most popular computational tools used for performing electronic structure calculations is the Kohn-Sham (KS) construction [2] in density-functional theory (DFT) [3], where the many-body Hamiltonian is mapped onto an effective mean-field auxiliary problem. Although the independent electron approximation is successful in describing crucial differences between transition metals, semiconductors and insulators [4], the method can fail for entire classes of materials.

A notable example is strongly correlated compounds where the electronic correlation is known to lead to interesting phenomena, such as high temperature superconductivity in cuprates [5] or even Mott insulating behavior [6]. These materials can be defined as systems that preserve the complexity of atomic-scale physics while in crystalline state, which usually happens in the presence of ions with localized open  $d$  and  $f$  shells [7, 8]. In this context, the mean-field KS description is inefficient, predicting metallic behavior for many transition-metal oxides that are experimentally reported as paramagnetic insulators, for instance [9].

Another issue is the band gap problem, where DFT significantly underestimates the electronic band gap of semiconductors and insulators [10]. In principle, this property could be exactly obtained from the ionization energy and electron affinity as  $E_{\text{gap}} = E(N_e + 1) + E(N_e - 1) - 2E(N_e)$  [7, 10], where  $N_e$  is the number of electrons. However, in the KS framework, the  $E_{\text{gap}}^{KS}$  is the difference between the highest occupied and lowest unoccupied states, which can largely differ from  $E_{\text{gap}}$ , due to discontinuities in the DFT potential [7, 10], specially for semiconductors and also strongly correlated systems [7].

Under these conditions, several approaches have been employed to correct or improve DFT band gap predictions, from the use of Wannier functions [11], to hybrid exchange-correlation functional [12, 13] and many-body perturbation theory based on GW methods [14]. DFT+U+V, based on the Extended Hubbard model [15], is also a robust strategy to treat the inadequate description of the local Coulomb interaction with the mean-field addition of  $U$  and  $V$  parameters [16]. Traditionally, the estimation of the Hubbard parameters was empirical. Only in the last decade an implementation was developed to compute them self-consistently [16, 17]. Although, the application of DFT+U or DFT+U+V can improve standard DFT predictions, as a few works have shown, the band gap outcome can depend on the Hubbard projector type used still yielding band gaps that are smaller than their respective experimental values [18].

An interesting alternative to the first-quantized DFT framework is to describe the electronic structure of crystals using fermionic lattice Hamiltonians such as the Extended Hubbard model, with previous applications ranging from polyacetylene [19], organic conductors [20], twisted bilayer graphene [21], and most notoriously, high-temperature superconductors [22]. A considerable limitation of the lattice description is the computational overhead of numerical simulations, with exact solutions being possible only for systems with a few particles [23]. As approximate methods, both Quantum Monte Carlo (QMC) [24] and Density Matrix Renormalization Group (DMRG) [25] have been extensively employed for simulating ground states of lattice systems, but each of these methods has its optimal range of application limited to specific use cases. Quantum Monte Carlo is known to be efficient and precise for bosons, but suffers from the “sign problem” when applied to fermions [26, 27]. Alternatively, while DMRG is successful in describing 1D [28] and 2D [23] lattices, the scaling of computational resources can be an issue for the 3D case [29].

It is natural to consider quantum computing algorithms for tackling simulations of lattice systems. The inherent quantum nature of the simulated systems makes the scaling of resources more favorable, and by considering a fully quantum description we are able to bypass approximations usually employed in mean-field and perturbative approaches. Moreover, there is a variety of proposals to tackle problems in materials science with quantum algorithms [1], with an extensive research effort investigating problem instances in which a provable quantum advantage can be achieved. [30]. However, the reduced scale and large amounts of hardware noise of modern-day quantum processors have so far limited the range of application to small systems with little industrial and technological relevance [31].

In the face of these challenges, the Sample-Based Quantum Diagonalization (SQD) framework [32] was proposed as an alternative for describing the spectra of fermionic systems. As part of a quantum-centric computing workflow, SQD leverages the capabilities of quantum computers as well as high-performance computing (HPC) environments, and it has proven successful in predicting both ground and excited state properties of quantum systems [33] with precisions that match the ones coming from classical state-of-the-art methods, for problem sizes of up to 40 spin orbitals [32]. So far, SQD applications have been restricted to quantum chemistry problems (isolated molecules).

In this contribution, we propose a general, *ab initio* framework for describing the electronic structure of crystalline materials with the Extended Hubbard Model. The lattice representation of the electronic Hamiltonian on solid crystals is obtained by means of a projection of the DFT electronic density onto a localized atomic basis set. Throughout this work, we consider bulk Silicon and Zirconia as use cases, due to the underestimation of the band gap by standard DFT. Next, we implement the SQD framework, in a novel application to crystalline solids, to compute the ground state energies of the constructed lattice Hamiltonians. Finally, we estimate the band gap of the semiconductor materials considered here, using the computed ground state energies, to compare with experimental results and the DFT+U+V mean-field approach. We show that while the methodology proposed here presents the same level of accuracy as DFT+U+V for Silicon, the quantum model improves the band gap prediction for Zirconia reaching excellent agreement with experimental results.

## Results

### Lattice Hamiltonian for crystals

A necessary step in any quantum simulation workflow is to obtain a Hamiltonian representation that correctly describes the properties of the physical system of interest. Here, we propose a self-consistent approach based on DFT for modeling periodic materials with lattice Hamiltonians. The workflow starts with a projection of the DFT electronic structure onto a localized basis set to obtain a tight-binding Hamiltonian whose band-structure matches the one computed via DFT (see Methods and Supporting Information). In this representation, the lattice sites are associated with atomic orbitals in each atomic site present in the structure used in the DFT calculation. Throughout this work, we have considered the valence atomic orbitals in the DFT pseudopotential as basis set (the electronic configurations are provided in the Methods section), thus each lattice site of the Hamiltonian is mapped to a single orbital from that set. It is important to notice that, in the proposed picture, orbitals coming from the same atom will be mapped into distinct lattice sites, as illustrated on [Figure 1](#). To include electronic correlations in the otherwise trivially solvable tight-binding Hamiltonian, we add intra-site and inter-site Hubbard interaction parameters that are also computed self-consistently via DFT, following the standard DFT+U+V framework [16, 17] (see Methods).

After adding the interaction terms, we obtain the Extended Hubbard Hamiltonian to describe the electrons in the solid crystal at each point of the  $\mathbf{k}$ -grid. Throughout this work, the lattice Hamiltonian is constructed only at the  $\Gamma$ -point, but the description is general for any point on the reciprocal space. The expression for the Hamiltonian (omitting the  $\mathbf{k}$ -point index) is given by

$$\hat{H} = \sum_{pq,\sigma} t_{pq} \hat{a}_{p,\sigma}^\dagger \hat{a}_{q,\sigma} + \sum_p U_p \hat{n}_{p,\uparrow} \hat{n}_{p,\downarrow} + \sum_{pq,\sigma\tau} V_{pq} \hat{n}_{p,\sigma} \hat{n}_{q,\tau}, \quad (1)$$

where  $t_{pq}$  are the hopping parameters between lattice sites (localized atomic orbitals, in our case) that were obtained via projection of the DFT electronic structure,  $U_p$  and

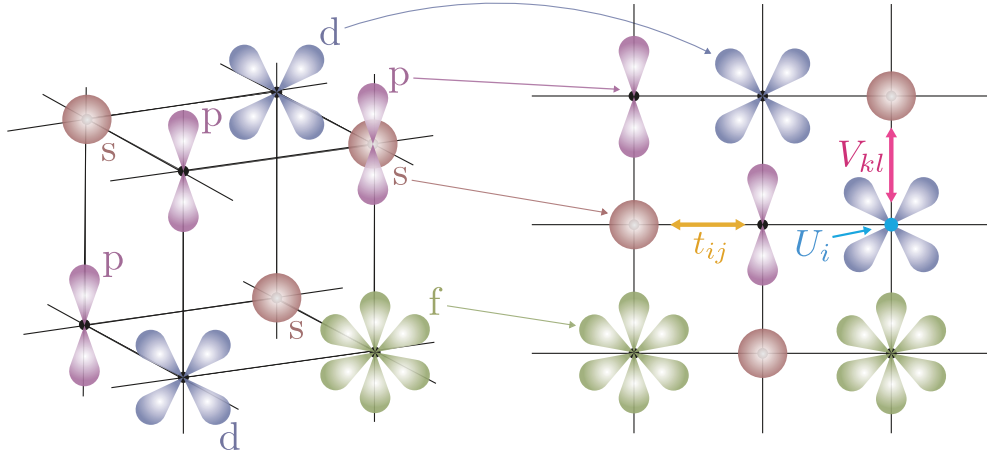


**Fig. 1** Diagram describing our framework to build a self-consistent lattice Hamiltonian for crystals. This involves projecting the electronic density obtained from a DFT calculation onto a localized basis set, which gives us an effective tight-binding Hamiltonian represented by a set of hopping parameters  $t_{ij}$ . We also add intra-site ( $U_i$ ) and inter-site ( $V_{kl}$ ) interaction parameters to the Hamiltonian that are calculated self-consistently as part of the DFT+U+V framework. The final Hamiltonian has the structure of the Extended Hubbard Hamiltonian, as shown in Equation 1. Here, each atomic orbital of each atom of the crystal is mapped to a single site in the projected lattice, as illustrated in the figure for a generic solid with a cubic lattice.

$V_{pq}$  are the standard intra-site and inter-site Hubbard interaction parameters obtained self-consistently,  $\{\hat{a}_{p\sigma}, \hat{a}_{p\sigma}^\dagger\}$  are the fermionic operators representing an atomic orbital  $p$  with spin  $\sigma$ , and we denote the respective number operators as  $\hat{n}_{i\sigma} \equiv \hat{a}_{i\sigma}^\dagger \hat{a}_{i\sigma}$ . The purpose of describing crystals using the quantum model in Equation 1 is to better access the electronic correlation effects that DFT fails to predict due to its mean-field character.

We now verify the usefulness of the proposed lattice representation for predicting physical properties when compared with DFT. As a metric for comparison, we consider the direct band gap evaluated at the  $\Gamma$ -point, which can be easily computed from the DFT electronic structure as well as from the proposed lattice representation. For any given solid with a Hamiltonian given by Equation 1, we can compute the band gap with the ground state energies evaluated in the symmetry sectors of the Hamiltonian with  $N_e - 1$ ,  $N_e$  and  $N_e + 1$  electrons [34], where  $N_e$  is the total number of electrons in the unit cell of the crystal. More details on the estimation of the band gap in the lattice representation can be found in the Methods section.

As use cases to perform the comparison we choose Silicon bulk (Si) and cubic Zirconia ( $\text{ZrO}_2$ ) solids, with the number of electrons and orbitals for both materials shown in the left panel of Figure 2. Although the traditional application of DFT+U or DFT+U+V is oriented towards transition metals with localized orbitals, its use has shown improvement in the band gap prediction of both Silicon and Zirconia. Campo *et al.* argues that, opposite to strongly correlated cases, Silicon bulk is a “strongly hybridized” system, where  $s$  and  $p$  orbital hybridization, intra-site, inter-site and intra-site, plays an important role for the electronic structure [16]. The authors also have

shown a good agreement to experimental results regarding the band gap prediction through the addition of  $U$  and  $V$  values calculated self-consistently. On the other hand, Zirconia is a transition metal oxide, a typical class of material that presents strong electronic correlations. However, the localized  $d$  orbitals have an occupation of zero due to the Zr oxidation state, indicating that applying the Hubbard correction might not be necessary [35]. Besides, since standard DFT already results in a wide band gap (although smaller than the experimental one), unless optical properties are the investigation focus, treating Zirconia at the level of standard DFT theory without any corrections is usually justified [35]. Despite of this fact, Gebauer shows that applying DFT+ $U$ , both in Zr and O, leads to band gap predictions in excellent agreement with experimental results [35], improving over standard DFT.

To highlight the differences in predictions between the two representations, we show the results for the band gap considering different amounts of electronic interaction, namely, the case with no interaction (pure tight-binding), only intra-site interactions, only inter-site interactions, and considering all interactions (extended Hubbard model). In the DFT calculations, we have also added intra-site and inter-site interactions using the DFT+ $U$ + $V$  framework, and for the comparison with the Lattice representation we have considered the same amount of interaction in both levels of theory to ensure a fair comparison.

In the case of Silicon, to disregard algorithmic errors in the prediction of the band gap we exactly diagonalize the lattice Hamiltonian with the full-configuration interaction (FCI) method. For the case of Zirconia, for which the FCI space is too large to allow an exact diagonalization, we have used the Heat-Bath Configuration Interaction (HCI) [36] method instead. We also add experimental estimates for the band gap of the considered materials for reference.

We show the results for the band gap estimation at  $\Gamma$  in Figure 2. We can see that for the case of Silicon, in both methods, the addition of electronic interaction does not improve the prediction towards the experimental value, and the difference between the predictions from DFT and the lattice representation is mild. It is important to highlight here, that while the inter-site  $V$  interaction between  $s$  and  $p$  orbitals was added, intra-site  $V$  couplings were not included since the methodology used here does not allow the computation of  $V$  values for intra-site manifolds. The lack of this coupling can indicate why the band gap was not improved in our work, opposite to the work of Campo *et. al.* [16].

Alternatively, for the case of Zirconia we have quantitatively different predictions when we compare both methods. We can see that at DFT level, the intra-site interaction parameter is responsible for the shift on the band gap (in relation with the non-interacting case), but in the lattice representation the inter-site interaction plays the dominant role. Even though, Zr  $d$  orbitals are empty, the application of DFT+ $U$  is expected to shift  $d$  states (conduction band) modifying the band gap. Interestingly, the lattice representation presents an opposite behavior, where the inter-site interaction is responsible for the band gap shift. This indicates fundamental methodological differences between both methods, suggesting that the lattice representation might present advantages for other materials as well.

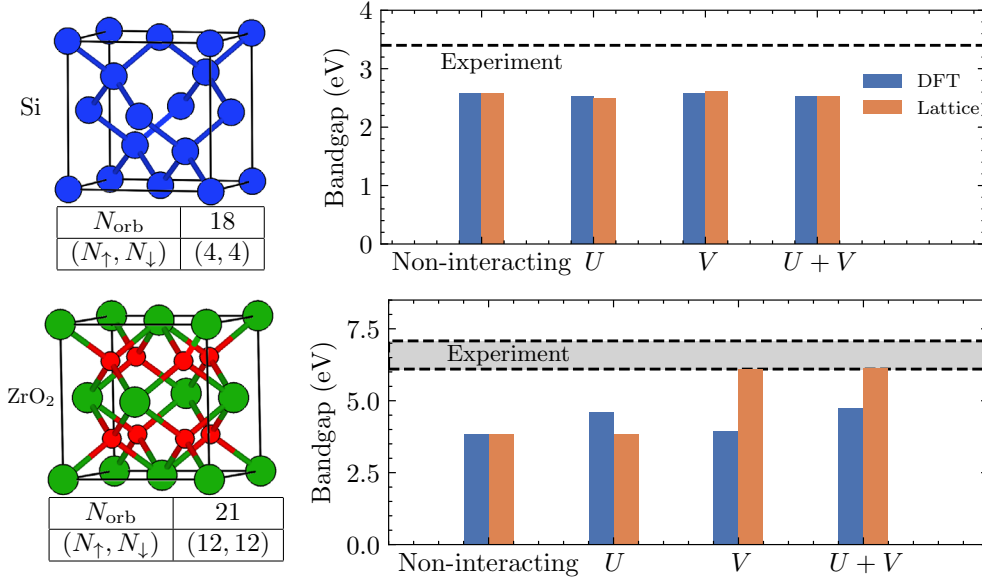


**Fig. 2** Comparison of the prediction of the direct band gap at the  $\Gamma$ -point for Silicon and Zirconia between DFT and the lattice Hamiltonian, considering different amounts of electronic interaction. We consider the cases of non-interacting electrons, just intra-site interactions (indexed as  $U$ ), just inter-site interactions ( $V$ ), and both intra-site and inter-site at once ( $U + V$ ). For the Silicon calculation, we exactly diagonalized the lattice Hamiltonian with the FCI method and for Zirconia we have used the HCI method. For comparison, we have added experimental predictions for the direct band gap, namely, the value of 3.40 eV given in [37] for Silicon and the range of 6.1-7.08 eV given in [38] for Zirconia. We also show orbital and electron count, as well as the unit cell for both materials.

In Table 1 we show a summary of past band gap predictions for Zirconia, showing also the values obtained from our method (considering the HCI result shown in Figure 2). We emphasize that, while our approach is built upon a DFT calculation, it produces quantitatively distinct predictions compared to standard DFT results. This is likely associated with the capability of our proposed quantum model to access correlation effects that are otherwise neglected in mean-field approaches such as DFT.

Method		Direct band gap (eV)
OLCAO [38]	Theory	4.9
LDA [39]	Theory	3.6
GW [39]	Theory	5.8
OLCAO [40]	Theory	3.8
DFT [41]	Theory	3.9
<b>This work</b>	Theory	<b>6.1</b>
Vacuum UV Spectroscopy[38]	Experiment	6.1,7.1

**Table 1** Direct band gap of ZrO<sub>2</sub> as obtained by previous works, compared this work. For our contribution we consider the value obtained from HCI, also shown in Figure 2.

## Quantum simulation of the lattice Hamiltonian

With the proposed lattice representation for periodic solids, it is possible to describe both the dynamics and the spectra of these systems using a variety of methods known in the literature. We perform a quantum-centric simulation to compute the ground state energy of the lattice Hamiltonian representing Silicon bulk on different electron-number symmetry sectors and, with these energies, we are able to estimate the associated band gap as described previously. We also present simulation results for the ground state of the Extended Hubbard Hamiltonian representing Zirconia. To compute the mentioned ground state energies, we apply the SQD framework [32] on the `ibm_torino` superconducting device (for more details on the hardware implementation, please refer to the Methods section). Even though the SQD framework was originally proposed for isolated molecules, here we apply it to a periodic lattice Hamiltonian. This can be done because we can map the Extended Hubbard Hamiltonian onto a general electronic Hamiltonian by a simple operation, that is described in detail in the Supporting Information.

The SQD framework is a configuration interaction (CI) method that consists in classically diagonalizing the Hamiltonian in the subspace spanned by electronic configurations (Slater determinants) sampled from a quantum device. The complete SQD workflow is described in the Methods, as well as in [32]. The circuit used for sampling the configurations must prepare a state that approximates the true ground state’s wavefunction, and for our calculations we have considered the LUCJ ansatz [42], a physically-inspired variational ansatz for electronic structure problems. The LUCJ ansatz used in this work can be represented as:

$$|\Psi\rangle = e^{\hat{K}_R} \prod_{\mu=1}^L e^{\hat{K}_\mu} e^{i\hat{J}_\mu} e^{-\hat{K}_\mu} |\mathbf{x}_o\rangle, \quad (2)$$

where  $\hat{K}_\mu = \sum_{pq,\sigma} K_{pq}^\mu \hat{a}_{p\sigma}^\dagger \hat{a}_{q\sigma}$  are one-body operators that generate orbital rotations,  $\hat{J}_\mu = \sum_{pq,\sigma\tau} J_{pq,\sigma\tau}^\mu \hat{n}_{p\sigma}^\dagger \hat{n}_{q\tau}$  are density-density operators between orbitals associated with adjacent qubits on the device (considering the Jordan-Wigner mapping), and  $|\mathbf{x}_o\rangle$  is the initial Hartree-Fock (HF) state. The variational parameters of the ansatz, namely  $K_{pq}^\mu$  and  $J_{pq,\sigma\tau}^\mu$ , are derived from the one- and two-body amplitudes coming from a Coupled-Cluster Singles and Doubles (CCSD) calculation, thus bypassing the need for a costly variational optimization. As usual for SQD implementations, the circuit is built on the molecular orbital basis, but in this work we have added an additional orbital rotation  $e^{\hat{K}_R}$  to rotate the prepared state to the atomic orbital basis before measuring. More information on the change of basis can be found on the Supporting Information. As classical benchmarks for our SQD results, we have considered the restricted HF (RHF), CCSD, FCI and HCI levels of theory.

In [Figure 3](#) we show the SQD results for the simulation of Silicon bulk. We have computed the ground state energies in the  $(N_\uparrow, N_\downarrow) = \{(4, 3), (4, 4), (5, 4)\}$  electron subspaces, where  $(N_\uparrow, N_\downarrow)$  are the number of spin up and down electrons, respectively. For this calculation we have considered both intra-site and inter-site interactions. We can see that in all three calculations the ground state energy estimates are within

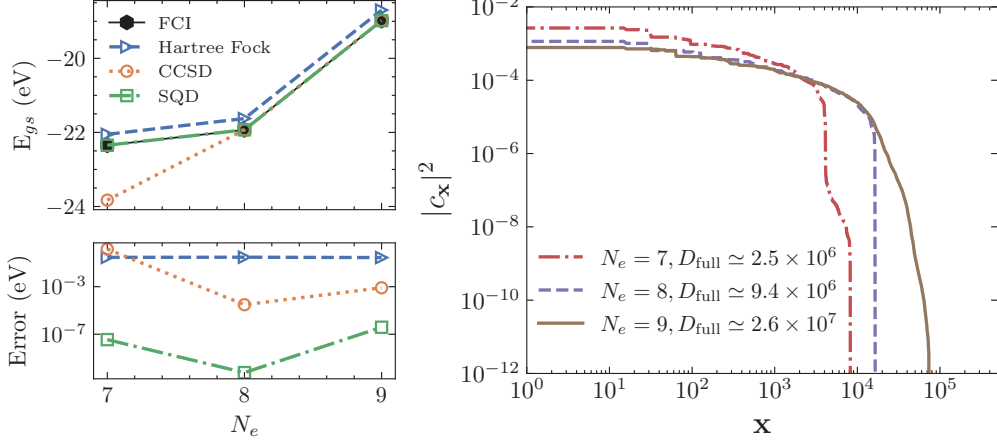


**Fig. 3** (Left) Ground state energy ( $E_g$ ) of Silicon bulk in the  $(N_{\uparrow}, N_{\downarrow}) = \{(4, 3), (4, 4), (5, 4)\}$  electron subspaces, with total number of electrons  $N_e = \{7, 8, 9\}$ , considering the Hamiltonian from Equation 1, in the case with all possible electronic interaction (inter-site and intra-site) computed using the SQD simulation framework as well as other classical methods used as benchmarks. We also show the energy difference (in eV) between each estimate and the FCI method, which accounts for the exact solution. These results were obtained from a 38-qubit experiment on the `ibm_torino` quantum processor. (Right) Probability amplitudes of the ground state obtained with SQD for the three symmetry sectors considered. Here,  $\mathbf{x}$  represents the index of the Slater determinants, arranged in decreasing order of the probabilities. The numbers of configurations used in the diagonalization which determine the memory cost of the calculation were  $d = \{4.4 \times 10^5, 1.5 \times 10^6, 6.8 \times 10^6\}$  for the  $N_e = \{7, 8, 9\}$  calculations, respectively, and the total Hilbert space dimension is indicated as  $D_{\text{full}}$ .

$10^{-5}$  eV of the exact value, surpassing the accuracy given by CCSD. We highlight how the SQD framework allows us to obtain accurate estimates on the system’s properties even in the presence of hardware noise. We also show the probability amplitudes of the quantum-selected ground state for the three symmetry sectors, considering the ground state written as  $|\Psi_{gs}\rangle = \sum_{\mathbf{x}} c_{\mathbf{x}}|\mathbf{x}\rangle$ , where  $\mathbf{x}$  indexes the Slater determinants, ordered according to the probabilities. We can see that that in all three cases the ground state obtained with SQD has non-negligible probability amplitudes on a number of configurations that is two orders of magnitude smaller than the complete Hilbert space dimension. We also show the dimension of the full Hilbert space of the system, to highlight that the selection of the configuration space given by SQD allows us to describe the system in a vector space considerably smaller than the one that would be considered in an exact diagonalization.

In Figure 4, we show the SQD results for Zirconia, which were obtained from a 46-qubit experiment on `ibm_torino`, and also from noiseless simulations. We compare the occupancies of the ground state over the considered atomic orbitals between DFT, DFT+U+V, and SQD. By inspecting the occupancies, we can see that adding the interaction parameters at the DFT level of theory does not affect the occupancy considerably, with only a slight shift in occupancy between the  $4d$  orbitals of Zirconium to the  $2p$  orbitals of the Oxygen atoms. Interestingly, in the SQD case, we see a starker

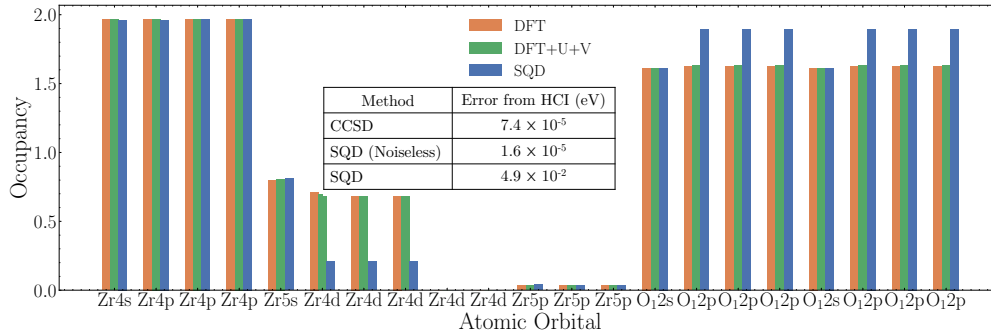


**Fig. 4** Occupancies of the ground state of Zirconia for  $N_e = 24$  electrons obtained from DFT, DFT+U+V and SQD. The SQD occupancy was obtained from data collected from the `ibm_torino` processor. We can see that adding the interaction parameters has a greater effect on the occupancy in the case of SQD. (Inset) Error with respect to HCI of the ground state energies obtained from noiseless SQD simulations, SQD on hardware, and CCSD. In the noiseless SQD case, the prediction is able to improve the energy prediction over CCSD, and in the hardware SQD case, the prediction is within chemical accuracy ( $\leq 50$  meV) of the HCI result.

shift in occupancy between the *Zr-4d* and *O-2p* atoms. This difference in the occupancies is likely related to the better estimate of the band gap shown in Figure 2. For the remaining orbitals the three methods predict very similar occupancies. In the Supporting information, we show that even though the energy prediction differs between the noiseless and noisy cases, the SQD occupancies obtained match almost exactly. Thus, we can safely disconsider the effects of hardware noise when inspecting the presented occupancy results.

We also show a table (Figure 4 inset) with the error of the ground state energy with respect to HCI obtained from different methods, namely, SQD sampled on a quantum device, SQD sampled from noiseless simulations and CCSD. Using HCI as our classical benchmark, we can see that both SQD and noiseless SQD are within chemical accuracy ( $\leq 50$  meV) of the HCI prediction, and for the noiseless case we were able to improve over the CCSD energy value, even though this value differs from HCI by only tens of  $\mu\text{eV}$ . For the noiseless case, the number of configurations used in the diagonalization (see Methods Section) was  $d = 1.3 \times 10^8$ , while for the calculation performed on hardware we had  $d = 1.8 \times 10^9$ . The full Hilbert Space size is  $D_{\text{full}} = 8.6 \times 10^{10}$ . In the noiseless case we obtain a better accuracy with a smaller number of configurations considered, therefore we see that the efficiency of sampling useful determinants decreases as a consequence of hardware noise.

## Discussion

We have developed an *ab initio* framework to describe crystalline solids, which allows us to build lattice Hamiltonian descriptions to correctly predict physical properties of these systems. We have applied our methodology to two materials, Silicon and Zirconia, and for the case of Zirconia we have obtained estimates for the band gaps that are in agreement with the experimental result given in Ref. [38], which was obtained with Vacuum Ultraviolet Spectroscopy.

The experimental band gap of Zirconia exhibits significant variation due to the influence of different growth techniques and conditions on the physical and chemical properties of this oxide [43]. Theoretical approaches have been used in the estimation of the band gap, with values ranging from 3.3 eV [44], with the use of the Local Density Approximation (LDA) [45] as exchange-correlation functional, to 5.8 eV within the GW methodology [39]. Despite of the fact that the GW methodology presents an excellent performance with respect to experimental results, there is a large computational cost associated [46]. In this work, owing to the small size of Silicon and Zirconia unit cells, the first-principles calculation of  $U$  and  $V$  along with the quantum model procedure is relatively fast, producing comparable results to GW using less computational resources.

We have applied a quantum-centric supercomputing scheme to simulate the ground state of the systems described by our framework. On pre-fault-tolerant quantum processors, we were able to obtain precise estimations of the ground state energies of the considered systems with minimal error mitigation overhead. This makes evident the usefulness of the SQD framework to extract meaningful results from present-day quantum processors.

We also highlight that our approach is general for any periodic material. While the proposed band gap estimation method is only relevant for semiconductors and insulators, one could in principle use our framework to study the ground state properties of conductors and superconductors. Our method is also scalable as we consider more complex materials, with the main computational bottleneck being the (classical) diagonalization algorithm. As the capabilities of both quantum and classical approaches to tackle this calculation evolves over time it will be possible to analyze materials with even more relevant industrial and technological applications.

## Methods

### Density Functional Theory and lattice projection

To obtain the electronic density of the ground state, the Quantum Espresso (QE) software [47–49] is used to perform electronic structure calculations through density functional theory (DFT) [2, 3]. Here, Si bulk is simulated with an FCC structure, an electronic valence configuration of  $3s^23p^23d^0$  and an optimized lattice parameter of 5.46 Å, in agreement with experimental results (5.43 Å) [50]. We used a Perdew-Burke-Ernzerhof (PBE) norm-conserving Martins-Troullier GIPAW [51] pseudopotential available in the QE pseudopotential database [52] as `Si.pbe-mt.gipaw.UPF`, with a kinetic energy cutoff for wavefunctions and charge density of 50 Ry and 200 Ry, respectively. It is worth noting that the inclusion of  $d$  orbitals in the valence bands was essential to later perform the tight-binding projection (see more details regarding the pseudopotential choice in the Supporting Information). The geometry optimization was performed with a force convergence threshold of  $5 \times 10^{-4}$ , while the electronic self-consistent convergence threshold was set to  $10^{-7}$  eV, with a  $8 \times 8 \times 8$   $\mathbf{k}$ -grid.

Similarly, Zirconia bulk was simulated with a FCC structure and optimized lattice parameter of 5.12 Å for the conventional unit cell in excellent agreement with experimental results (5.13 Å) [53]. The electronic valence configuration for Zr and O

are  $4s^24p^64d^25s^2$  and  $2s^22p^4$ , respectively. The pseudopotentials used were from the SSSP PBE Efficiency v1.3.0 package [54], with a kinetic energy cutoff for wavefunctions and charge density of 80 Ry and 320 Ry, respectively, which are larger than the ones suggested by the SSSP library. The geometry optimization was performed with the same parameters used for Silicon with the exception of the  $\mathbf{k}$ -grid of  $6 \times 6 \times 6$ .

The intra-site  $U$  and inter-site  $V$  Hubbard parameters are also computed with QE in the self-consistent DFT+U+V framework according to the implementation of density functional perturbation theory [16, 17]. Initial guesses for  $U$  and  $V$  ( $10^{-8}$  eV) are provided as input to the self-consistent step, using orthogonalized atomic orbitals as Hubbard projectors. We considered  $U_{3p}$  and  $V_{3p-3s}$  for Silicon, and  $U_{4d}$  and  $V_{4d-2p}$  in the case of Zirconia.

The tight-binding representation is calculated by a projection of the plane-wave electronic structure from QE onto localized atomic orbitals through the use of the PAOFLOW software [55, 56]. The projection outcome is a representation of the electronic structure as a lattice Hamiltonian, expanded in the atomic orbital basis present in the pseudopotential used in QE, with its respective coefficients, i.e., hopping parameters. It is important to emphasize that the output from QE considered is the one from standard DFT, where we do not include the  $U$  and  $V$  corrections. The tight-binding projection effectively describes the material, reproducing accurately the DFT energy levels of the band structure, as shown in the Supporting Information.

## Quantum Computing

We describe in detail the Sample-Based Quantum Diagonalization (SQD) workflow we have employed to diagonalize the lattice Hamiltonians for the considered materials. For any given system described by an Extended Hubbard Hamiltonian given by Equation 1, the first step is to map the associated hopping and Hubbard interaction parameters to one- and two-body integrals of an effective electronic Hamiltonian (see Supporting Information). This enables us to apply methods from quantum chemistry to diagonalize the Hamiltonian, such as the Hartree-Fock, CCSD and FCI levels of theory. With this new electronic Hamiltonian representing the crystal, we perform a standard CCSD calculation using the chemistry software PySCF [57]. With the one- and two-body amplitudes resulting from this calculation, we build the LUCJ circuit as written in Equation 2 using `ffsim` [58]. In this work we consider a single layer of the ansatz ( $\mu = 1$  in Equation 2). The circuit layouts and parameters used in our simulations are presented in Figure 5.

Following the choice of basis of the DFT calculation, the Extended Hubbard Hamiltonian in Equation 1 is initially built in the atomic orbitals basis set. However, it is a standard procedure in quantum chemistry applications to work in the molecular orbitals basis, in which we can find the single-determinant state with the largest possible overlap with the exact ground state of the system. In the chemistry context, this particular electronic configuration is usually referred to as the Hartree-Fock state. Similarly, we also construct the first layer of the LUCJ circuit in the basis of molecular orbitals. However, in our case we include an additional orbital rotation at the end of the circuit to change the basis of the prepared state back to the atomic orbital basis. For both materials considered in this work (Silicon and Zirconia), we observed

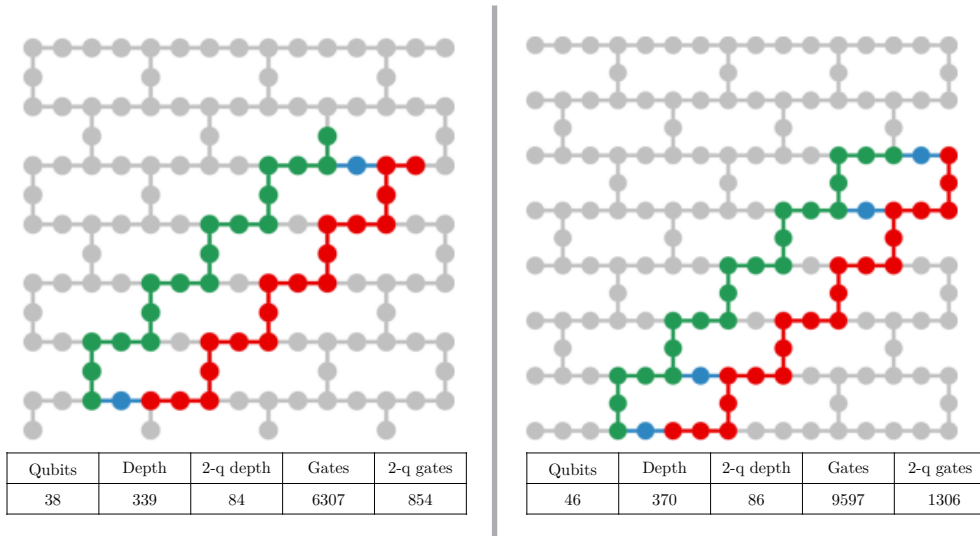


**Fig. 5** Layouts for the LUCJ circuits used to simulate the ground state of Silicon (Left) and Zirconia (Right) on the `ibm_torino` quantum processor. We also show relevant parameters of the circuit on the tables at the bottom.

an improvement in the precision and memory cost of the SQD calculations when considering this choice of basis, and we show a comparison between the results obtained using both basis sets in the Supporting information.

After preparing the circuits, we executed them on the `ibm_torino` quantum processor to collect a set of samples given by  $\{|\mathbf{x}\rangle\}$ , where  $\mathbf{x}$  are bitstrings. For each of the calculations considered we ran a total of  $2.5 \times 10^6$  shots on the device. Following the procedure discussed in [32], with the collected samples we construct  $K_b$  batches of  $d$  configurations, given by  $\mathcal{S}_{(k)} : k = 1, \dots, K_b$ . We proceed to diagonalize the Hamiltonian projected in the  $d$ -dimensional subspace spanned by the configuration in each batch. The projected Hamiltonian can be written as

$$\hat{H}_{\mathcal{S}^{(k)}} = \hat{P}_{\mathcal{S}^{(k)}} \hat{H} \hat{P}_{\mathcal{S}^{(k)}}, \quad \text{with } \hat{P}_{\mathcal{S}^{(k)}} = \sum_{\mathbf{x} \in \mathcal{S}^{(k)}} |\mathbf{x}\rangle \langle \mathbf{x}|.$$

We consider the final ground state energy result as the lowest energy found across all the batches. For the calculations of Silicon and Zirconia we have used  $K_b = 5$  and  $K_b = 1$ , respectively, and we considered different values of  $d$ , increasing them until convergence. The diagonalizations for both the SQD, FCI, and HCI calculations were performed using the Davidson algorithm as implemented in PySCF [57] and DICE [59]. We have used the implementation of the SQD and HCI workflows from `qiskit-addon-sqd` and `qiskit-addon-dice-solver` software packages.

In our hardware experiments, we have used Dynamical Decoupling as an error mitigation method [60], with standard configurations, as implemented in the Qiskit

library version 1.3.0 [61]. For the noiseless simulations, we have used the Approximate Quantum Compiling workflow for the simulation of circuits, presented in Ref. [62] and implemented in the `qiskit-addon-aqc-tensor` package [63].

## Band gap calculation

With the ground state energies obtained with SQD, we can estimate the band gap of the crystals associated with the projected Hubbard Hamiltonians. The band gap ( $E_g$ ) can be computed as a function of the ground-state energy of the Hamiltonian in the  $N_e$ ,  $N_e - 1$  and  $N_e + 1$  electron number symmetry sectors, according to the following function:  $E_g = E[N_e - 1] + E[N_e + 1] - 2E[N_e]$  [34], where  $E[N]$  is the ground-state energy of the Hamiltonian in the  $N$  electron symmetry sector. On the other hand, the DFT band gap has been calculated as the energy difference between the lowest unoccupied and highest occupied Kohn-Sham states in the band structure. Previous works have shown that although using the DFT energies is not suitable to obtain the band gap according to this methodology, other methods such as the direct random phase approximation (dRPA) [64] provide band gap estimations in good agreement with experiments [65]. Here, CCSD, FCI, and SQD ground state energies are utilized to obtain the Silicon and Zirconia band gaps. Despite of the methodological difference to compute the band gap, the use of the ground state energy function yields the same band gap result as the DFT computed ones for the tight-binding lattice Hamiltonian without the Hubbard parameters.

# Supporting information

## Mapping between lattice and electronic Hamiltonians

After projecting the DFT electronic structure onto a tight-binding Hamiltonian and including the  $U$  and  $V$  interaction parameters, we obtain an Extended Hubbard Hamiltonian, as written in Equation 1. Unlike in most discussions on the extended Hubbard model, here the hopping parameters and the inter-site interactions are not restricted to first or second neighbors in the lattice, but are rather determined by the DFT projection and therefore specific to each material. A non-zero hopping term between two orbitals, essentially means that they are considered as “neighbors”.

We now describe how to compute the ground state energy of the extended Hubbard Hamiltonian described in Equation 1 using the SQD framework, that was originally designed for quantum chemistry calculations of isolated molecules [32]. In the chemistry context, we describe the systems using a general electronic Hamiltonian in second quantization of the form

$$H_{chem} = \sum_{pq,\sigma} h_{pq} c_{p,\sigma}^\dagger c_{q,\sigma} + \frac{1}{2} \sum_{pqrs,\sigma\tau} h_{pqrs,\sigma\tau} c_{p,\sigma}^\dagger c_{r,\tau}^\dagger c_{s,\tau} c_{\sigma,q}, \quad (3)$$

where  $h_{pq}$  and  $h_{pqrs,\sigma\tau}$  are the one- and two-body tensors derived from the overlap and electronic repulsion integrals, respectively. Regarding the two-body tensor, for some fixed spatial orbital indices  $pqrs$  the tensor element  $h_{pqrs}$  can have different values depending on the spins being parallel or not, and that is why we also include the spin dependence on  $h_{pqrs,\sigma\tau}$ . Now observe that we can rewrite the extended Hubbard model in Equation 1 as a molecular Hamiltonian by making the following mappings:

$$h_{pq} \leftrightarrow t_{pq}, \quad (4)$$

$$h_{pppp,\sigma\tau} = U_p \quad (5)$$

$$h_{ppqq,\sigma\tau} = 2V_{pq} \quad (6)$$

$$h_{pppp,\sigma\sigma} = 0 \quad (7)$$

$$h_{pqrs,\sigma\tau} = 0 \text{ if } p \neq q \text{ or } r \neq s. \quad (8)$$

By looking at the two-body term in Equation 3 we can see that the creation and annihilation operators are in a different ordering as the ones in Equation 1, but we can reorder them by permuting the operators exactly twice, in such a way that the negative sign coming from the anti-commutation relations cancels out.

## Change of basis

When searching for the ground state of a molecular system in quantum chemistry, it is customary to describe the systems in the *molecular orbital* basis. One of the goals of this approach is to find the single Slater determinant state (electronic configuration) whose energy is closest as possible to the exact ground state of the system. In quantum computing applications in Chemistry, more specifically the ones that employ variational ansätze such as the LUCJ circuit, the mentioned change of

basis is extensively employed because in the Jordan-Wigner mapping the preparation of single determinant states requires only a single layer of CNOT gates applied to the molecular orbitals occupied in the associated configuration.

In our simulation workflow for periodic solids, since we are treating the lattice Hamiltonian in a molecular representation, it is also convenient to work in the molecular orbital basis, since we can prepare a initial state with minimal quantum cost overhead that gives a reasonable approximation of the exact ground state. However, differently from standard chemistry workflows, in our calculations we change the basis of the ansatz state back to the atomic orbital basis before the measurements. A general orbital rotation between two sets of  $N$  fermionic modes (in our case the operators associated with the atomic and molecular orbitals basis sets) can be defined in terms of a  $N \times N$  unitary matrix  $\mathcal{U}$ , that maps fermionic operators  $\{a_i, a_i^\dagger\}$  from one set to a linear combination of operators from the other set  $\{b_i, b_i^\dagger\}$  as  $a_i \rightarrow \sum_j \mathcal{U}_{ji} b_j$ . Conversely, to map state vectors between different sets of modes we can apply the  $2^N \times 2^N$  unitary matrix  $\mathcal{U} = \exp \sum_{ij} \log(\mathcal{U})_{ij} a_i^\dagger a_j$  directly to the state. In order to build the orbital rotation that changes the basis between the atomic and molecular orbitals basis sets we just set  $\mathcal{U}$  as the molecular orbital coefficient matrix, or the coefficients of the expansion of the molecular orbitals in terms of the atomic ones, that can be computed with standard chemistry software such as PySCF [57]. In the Jordan-Wigner mapping it is straightforward to map general orbital rotations into quantum circuit operations, and more details can be found in Ref. [58].

	Atomic Basis	Molecular Basis
<b>Energy (eV)</b>	-337.943	-321.483
<b>Error w.r.t. HCl (eV)</b>	$4.9 \times 10^{-2}$	$1.6 \times 10^1$
<b>Subspace Dimension</b>	$1.8 \times 10^9$	$3.5 \times 10^9$

**Table 2** Comparison between SQD results considering the two choices of basis, atomic and molecular. As a benchmark we have used the ground state energy results computed with HCl.

To highlight the advantages of performing the change of basis in our use cases, we show in Table 2 a comparison between the SQD results obtained for Zirconia, while considering the two choices of basis. These results were also obtained from the `ibm.torino` processor, and for the molecular basis case we have considered the truncated version of the LUCJ circuit, also employed in other works on SQD such as Ref. [32]. For the atomic basis case, we have not truncated the ansatz, because the final orbital rotation already prevents the vanishing parameter problem of the original LUCJ circuit. We have performed one SQD calculation for each choice of basis to obtain the ground state energies, and to make a fair comparison, in each calculation we have used a similar amount of memory ( $\sim 2.5$  Tb).

We show the value of the energy obtained from both calculations, as well as the error in the prediction when compared with HCl, and also the subspace dimensions considered in each of the diagonalizations, which can also be interpreted as the number of configurations present on the output ground state. We can see that in the molecular

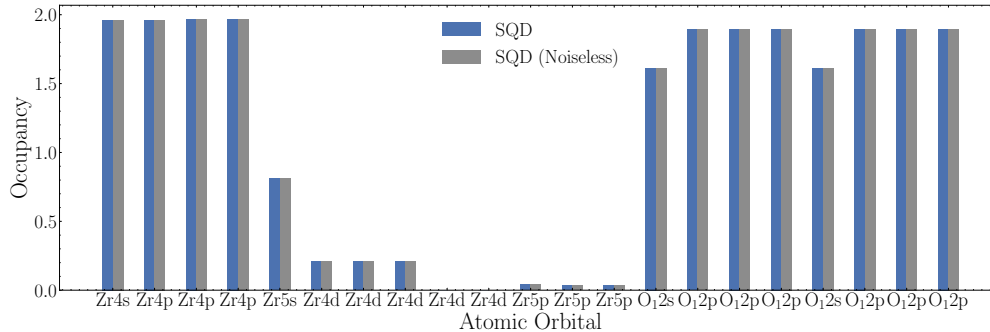


**Fig. 6** Occupancies of the ground state of Zirconia, obtained from sampling the quantum hardware as well as from noiseless simulations.

case, even though the number of configurations of the ground state is considerably larger, the precision in the energy is orders of magnitude away from the one given by the atomic basis calculation. From this we can see that the ground state is much more accurately represented in the atomic basis, with a reduced number of configurations considered.

### Comparing the occupancies in the hardware and noiseless simulation cases

In the main text, we present the occupancy obtained for Zirconia using the data obtained from `ibm_torino`. To highlight that the presented results are physically meaningful, here we compare the occupancies obtained in the noiseless and noisy case. In [Figure 6](#), it is clear that the presence of hardware noise does not affect the obtained occupancy considerably.

### Electronic structure and tight-binding projection

The computation of  $U$  and  $V$  values should be converged with respect to the Monkhorst-Pack grid  $\mathbf{q}$ -mesh, similarly to the  $\mathbf{k}$ -mesh in the ground state calculation. Here, the final values are computed in either a  $3 \times 3 \times 3$  or  $4 \times 4 \times 4$   $\mathbf{q}$ -grid, for Silicon and Zirconia, respectively. Only nonequivalent atoms by symmetry were perturbed (`find_atpert = 3`) and the convergence threshold for the response function  $\chi$  was set as  $10^{-7}$ . In both cases, the  $\mathbf{q}$ -mesh was tested for convergence with larger grids, resulting in a variation of the order of 0.01 and 0.001 eV for  $U$  and  $V$  values, respectively.

A comparison between the Quantum Espresso [47–49] and PAOFLOW [55, 56] band structures of each semiconductor investigated in this work is presented in [Figure 7](#). This comparison indicates an excellent performance of tight-binding projection executed by PAOFLOW, where the occupied and first unoccupied bands are accurately represented. Note that the match between DFT and PAOFLOW bands could be further enhanced, however, this is outside the scope of this work, which considers only the  $\Gamma$ -point.

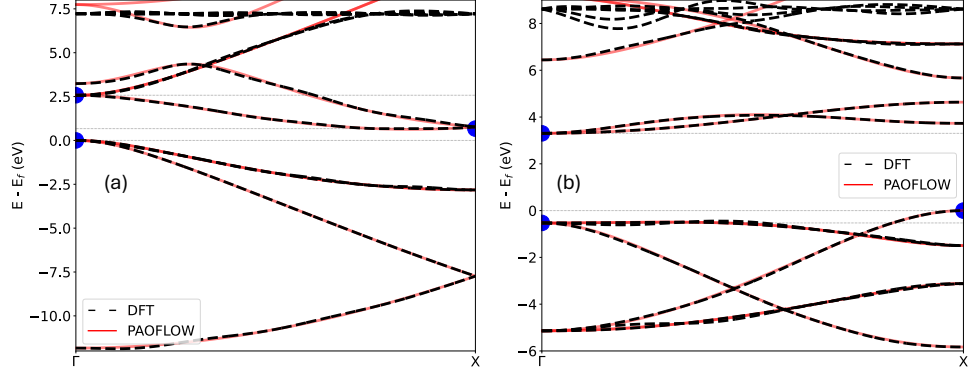


**Fig. 7** Band structure for (a) Silicon and (b) Zirconia. The Quantum Espresso results using standard DFT is in dashed black line and the PAOFLOW projection is in solid red line. The blue circles marks the highest occupied and lowest unoccupied states. This is also done for at the  $\Gamma$ -point to indicate the direct band gap.

A graphical visualization of the tight-binding Hamiltonian can be seen in [Figure 8](#) for Silicon and Zirconia. The color map represents the hopping parameters, indicating the interaction among atomic orbital sites. The matrix is divided in blocks, according to the site of each atom of the unit cell. Therefore, interactions within the diagonal and off-diagonal blocks are intra-site and inter-site couplings, respectively.

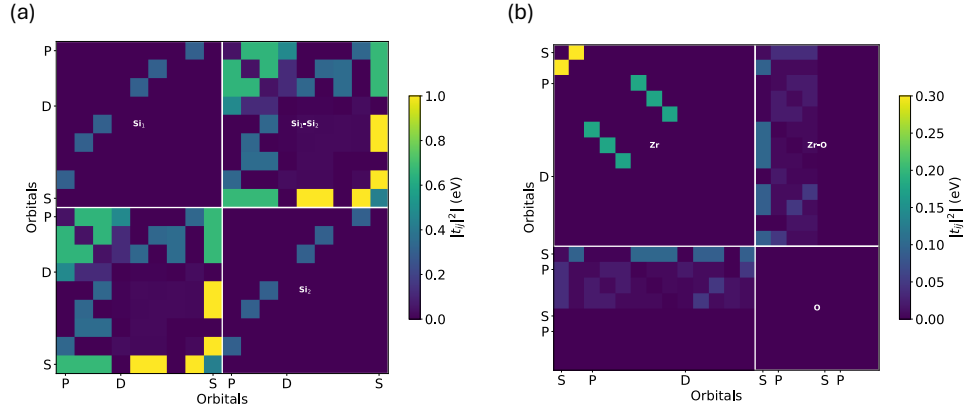


**Fig. 8** Graphical representation of the Hamiltonian at the  $\Gamma$ -point for (a) Silicon and (b) Zirconia. The color map represents the normalized squared value of the hopping ( $|t_{ij}|^2$ ) and the columns and rows are the localized orbital atomic basis. Note that for Zirconia, due to strong interactions from Zr  $s$  orbitals, the maximum normalized value shown has been set to  $0.3 \text{ eV}^2$  to facilitate the visualization of other interactions.

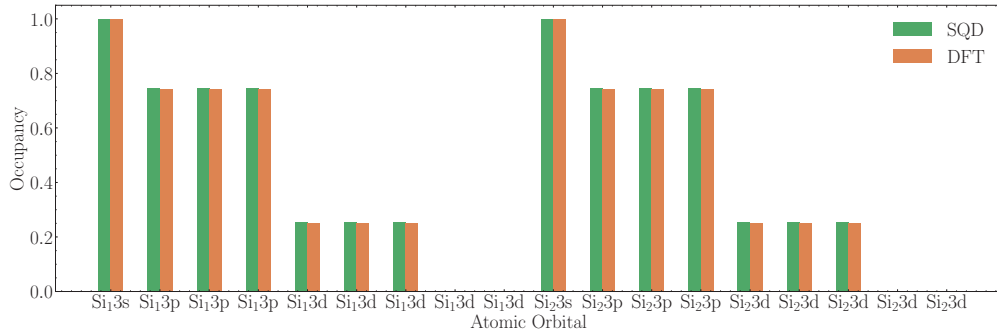


**Fig. 9** Occupancies of the ground state of Silicon, obtained from SQD and DFT, considering the non-interacting case where  $U = V = 0$ .

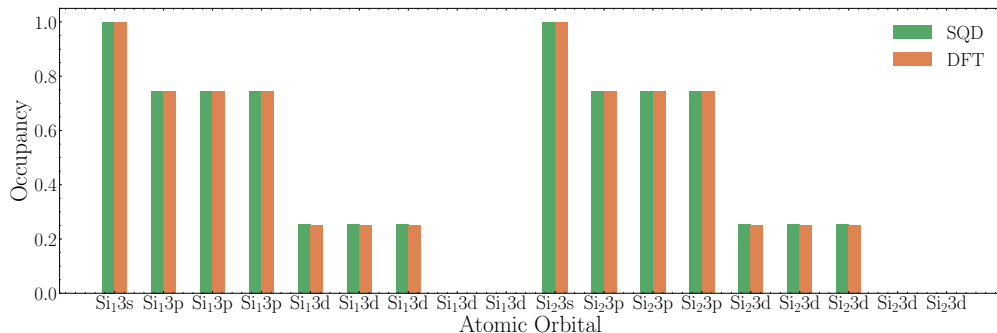


**Fig. 10** Occupancies of the ground state of Zirconia, obtained from SQD and DFT, considering the non-interacting case where  $U = V = 0$ .

## Comparing the occupancies between DFT and SQD for the non-interacting (tight-binding) case

In the case where the intra-site and inter-site parameters are set to zero, the Hubbard Hamiltonian reduces to a tight-binding Hamiltonian, where the only contribution comes from the hopping parameters. Since, in our workflow, the hopping parameters come from the projection of the DFT electronic structure, the ground state of the tight-binding Hamiltonian should (by construction) share the properties of the ground state found by DFT. In [Figure 9](#) and [Figure 10](#), we show a comparison between the occupancies of the ground state considering SQD and DFT, as a sanity check, just to show the consistency of the projection operation. The SQD results were obtained with noiseless simulations.

**Code Availability.** Here is a list of all the code repositories used in this work: Quantum Espresso [\[49\]](#), PAOFLOW [\[55\]](#), PySCF [\[57\]](#), `ffsim` [\[58\]](#), Qiskit SDK [\[61\]](#), `qiskit-addon-sqd` [\[66\]](#), `qiskit-addon-dice-solver` [\[67\]](#), `qiskit-addon-aqc-tensor` [\[63\]](#).

**Acknowledgments.** We would like to thank Mario Motta, Mirko Amico, Kevin Sung, Petar Jurcevic, Ieva Liepuoniute, Tanvi Gujarati, Ed Chen, Gavin Jones and

Javier Robledo Moreno (IBM) for enlightening discussions that helped this work. We would also like to acknowledge Ramon Cardias (CBPF) for introducing the PAOFLOW software to the group and Prof. Marcio Costa (UFF) for the fruitful discussions and guidance on the use of PAOFLOW.

## References

- [1] Alexeev, Y., Amsler, M., Barroca, M.A., Bassini, S., Battelle, T., Camps, D., Casanova, D., Choi, Y.J., Chong, F.T., Chung, C., Codella, C., Córcoles, A.D., Cruise, J., Di Meglio, A., Duran, I., Eckl, T., Economou, S., Eidenbenz, S., Elmegreen, B., Fare, C., Faro, I., Fernández, C.S., Ferreira, R.N.B., Fuji, K., Fuller, B., Gagliardi, L., Galli, G., Glick, J.R., Gobbi, I., Gokhale, P., Puente Gonzalez, S., Greiner, J., Gropp, B., Grossi, M., Gull, E., Healy, B., Hermes, M.R., Huang, B., Humble, T.S., Ito, N., Izmaylov, A.F., Javadi-Abhari, A., Jennewein, D., Jha, S., Jiang, L., Jones, B., Jong, W.A., Jurcevic, P., Kirby, W., Kister, S., Kitagawa, M., Klassen, J., Klymko, K., Koh, K., Kondo, M., Kürkçüoğlu, D.M., Kurowski, K., Laino, T., Landfield, R., Leininger, M., Leyton-Ortega, V., Li, A., Lin, M., Liu, J., Lorente, N., Luckow, A., Martiel, S., Martin-Fernandez, F., Martonosi, M., Marvinnay, C., Medina, A.C., Merten, D., Mezzacapo, A., Michielsen, K., Mitra, A., Mittal, T., Moon, K., Moore, J., Mostame, S., Motta, M., Na, Y.-H., Nam, Y., Narang, P., Ohnishi, Y.-y., Ottaviani, D., Otten, M., Pakin, S., Pascuzzi, V.R., Pednault, E., Piontek, T., Pitera, J., Rall, P., Ravi, G.S., Robertson, N., Rossi, M.A.C., Rydlichowski, P., Ryu, H., Samsonidze, G., Sato, M., Saurabh, N., Sharma, V., Sharma, K., Shin, S., Slessman, G., Steiner, M., Sitdikov, I., Suh, I.-S., Switzer, E.D., Tang, W., Thompson, J., Todo, S., Tran, M.C., Trenev, D., Trott, C., Tseng, H.-H., Tubman, N.M., Tureci, E., Valiñas, D.G., Vallecorsa, S., Wever, C., Wojciechowski, K., Wu, X., Yoo, S., Yoshioka, N., Yu, V.W.-z., Yunoki, S., Zhuk, S., Zubarev, D.: Quantum-centric supercomputing for materials science: A perspective on challenges and future directions. *Future Generation Computer Systems* **160**, 666–710 (2024) <https://doi.org/10.1016/j.future.2024.04.060>
- [2] Kohn, W., Sham, L.J.: Self-consistent equations including exchange and correlation effects. *Phys. Rev.* **140**, 1133–1138 (1965) <https://doi.org/10.1103/PhysRev.140.A1133>
- [3] Hohenberg, P., Kohn, W.: Inhomogeneous electron gas. *Phys. Rev.* **136**, 864–871 (1964) <https://doi.org/10.1103/PhysRev.136.B864>
- [4] Burke, K., Wagner, L.O.: Dft in a nutshell. *International Journal of Quantum Chemistry* **113**(2), 96–101 (2013) <https://doi.org/10.1002/qua.24259>
- [5] Bussmann-Holder, A., Keller, H.: High-temperature superconductors: underlying physics and applications. *Zeitschrift für Naturforschung B* **75**(1-2), 3–14 (2020) <https://doi.org/10.1515/znb-2019-0103>

- [6] Sachdev, S.: Understanding correlated electron systems by a classification of mott insulators. *Annals of Physics* **303**(1), 226–246 (2003) [https://doi.org/10.1016/S0003-4916\(02\)00024-6](https://doi.org/10.1016/S0003-4916(02)00024-6)
- [7] Pavarini, E.: Solving the strong-correlation problem in materials. *La Rivista del Nuovo Cimento* **44**(11), 597–640 (2021) <https://doi.org/10.1007/s40766-021-00025-8>
- [8] Solovyev, I.V.: Combining dft and many-body methods to understand correlated materials. *Journal of Physics: Condensed Matter* **20**(29), 293201 (2008) <https://doi.org/10.1088/0953-8984/20/29/293201>
- [9] Mandal, S., Haule, K., Rabe, K.M., Vanderbilt, D.: Systematic beyond-dft study of binary transition metal oxides. *npj Computational Materials* **5**(1), 115 (2019) <https://doi.org/10.1038/s41524-019-0251-7>
- [10] Schlüter, M., Sham, L.J.: Density-functional theory of the band gap. In: Löwdin, P.-O. (ed.) *Density Functional Theory of Many-Fermion Systems. Advances in Quantum Chemistry*, vol. 21, pp. 97–112. Academic Press, ??? (1990). [https://doi.org/10.1016/S0065-3276\(08\)60593-6](https://doi.org/10.1016/S0065-3276(08)60593-6)
- [11] Ma, J., Wang, L.-W.: Using wannier functions to improve solid band gap predictions in density functional theory. *Scientific Reports* **6**(1), 24924 (2016) <https://doi.org/10.1038/srep24924>
- [12] Perdew, J.P., Schmidt, K.: Jacob’s ladder of density functional approximations for the exchange-correlation energy. *AIP Conference Proceedings* **577**(1), 1–20 (2001) <https://doi.org/10.1063/1.1390175>
- [13] Tao, J., Perdew, J.P., Staroverov, V.N., Scuseria, G.E.: Climbing the density functional ladder: Nonempirical meta-generalized gradient approximation designed for molecules and solids. *Phys. Rev. Lett.* **91**, 146401 (2003) <https://doi.org/10.1103/PhysRevLett.91.146401>
- [14] Setten, M.J., Weigend, F., Evers, F.: The gw-method for quantum chemistry applications: Theory and implementation. *Journal of Chemical Theory and Computation* **9**(1), 232–246 (2013) <https://doi.org/10.1021/ct300648t>
- [15] Zhang, Y., Callaway, J.: Extended hubbard model in two dimensions. *Phys. Rev. B* **39**, 9397–9404 (1989) <https://doi.org/10.1103/PhysRevB.39.9397>
- [16] Leiria Campo, V., Cococcioni, M.: Extended dft + u + v method with on-site and inter-site electronic interactions. *Journal of Physics: Condensed Matter* **22**(5), 055602 (2010) <https://doi.org/10.1088/0953-8984/22/5/055602>
- [17] Timrov, I., Marzari, N., Cococcioni, M.: Hp – a code for the calculation of hubbard parameters using density-functional perturbation theory. *Computer Physics*

- Communications **279**, 108455 (2022) <https://doi.org/10.1016/j.cpc.2022.108455>
- [18] Naveas, N., Pulido, R., Marini, C., Hernández-Montelongo, J., Silván, M.M.: First-principles calculations of hematite ( $\alpha - Fe_2O_3$ ) by self-consistent dft+u+v. *iScience* **26**(2) (2023) <https://doi.org/10.1016/j.isci.2023.106033>
- [19] Kivelson, S., Su, W.-P., Schrieffer, J.R., Heeger, A.J.: Missing bond-charge repulsion in the extended hubbard model: Effects in polyacetylene. *Phys. Rev. Lett.* **58**, 1899–1902 (1987) <https://doi.org/10.1103/PhysRevLett.58.1899>
- [20] Castet, F., Fritsch, A., Ducasse, L.: Determination of the Coulombic Interaction Parameters of the Extended Hubbard Model in the Organic Conductors. *Journal de Physique I* **6**(4), 583–597 (1996) <https://doi.org/10.1051/jp1:1996231>
- [21] Da Liao, Y., Meng, Z.Y., Xu, X.Y.: Valence bond orders at charge neutrality in a possible two-orbital extended hubbard model for twisted bilayer graphene. *Phys. Rev. Lett.* **123**, 157601 (2019) <https://doi.org/10.1103/PhysRevLett.123.157601>
- [22] Luo, Z., Lv, B., Wang, M., Wú, W., Yao, D.-X.: High-*tc* superconductivity in  $La_3Ni_2O_7$  based on the bilayer two-orbital t-j model. *npj Quantum Materials* **9**(1), 61 (2024) <https://doi.org/10.1038/s41535-024-00668-w>
- [23] Liang, S., Pang, H.: Approximate diagonalization using the density matrix renormalization-group method: A two-dimensional-systems perspective. *Phys. Rev. B* **49**, 9214–9217 (1994) <https://doi.org/10.1103/PhysRevB.49.9214>
- [24] Ceperley, D.M., Alder, B.J.: Ground state of the electron gas by a stochastic method. *Phys. Rev. Lett.* **45**, 566–569 (1980) <https://doi.org/10.1103/PhysRevLett.45.566>
- [25] White, S.R.: Density matrix formulation for quantum renormalization groups. *Phys. Rev. Lett.* **69**, 2863–2866 (1992) <https://doi.org/10.1103/PhysRevLett.69.2863>
- [26] Troyer, M., Wiese, U.-J.: Computational complexity and fundamental limitations to fermionic quantum monte carlo simulations. *Phys. Rev. Lett.* **94**, 170201 (2005) <https://doi.org/10.1103/PhysRevLett.94.170201>
- [27] Pan, G., Meng, Z.Y.: The sign problem in quantum Monte Carlo simulations, pp. 879–893. Elsevier, ??? (2024). <https://doi.org/10.1016/b978-0-323-90800-9.00095-0> . <http://dx.doi.org/10.1016/B978-0-323-90800-9.00095-0>
- [28] Sobczak, P., Barasiński, A., Drzewiński, A., Kamieniarz, G., Kłak, J., Bieńko, A., Mroziński, J.: Magnetic properties and dmrg modeling of the 1d bimetallic thiocyanate bridged compound  $(CuL_1)[Co(NCS)_4]$  (11=*n*-rac-5,12-me2-[14]-4,11-dienen4). *Polyhedron* **28**(9), 1838–1841 (2009) <https://doi.org/10.1016/j.poly.2009.01.031> . Proceedings of the 11th International Conference on Molecule-based

- [29] Mezzacapo, F., Schuch, N., Boninsegni, M., Cirac, J.I.: Ground-state properties of quantum many-body systems: entangled-plaquette states and variational monte carlo. *New Journal of Physics* **11**(8), 083026 (2009) <https://doi.org/10.1088/1367-2630/11/8/083026>
- [30] Wu, D., Rossi, R., Vicentini, F., Astrakhantsev, N., Becca, F., Cao, X., Carrasquilla, J., Ferrari, F., Georges, A., Hibat-Allah, M., Imada, M., Läuchli, A.M., Mazzola, G., Mezzacapo, A., Millis, A., Robledo Moreno, J., Neupert, T., Nomura, Y., Nys, J., Parcollet, O., Pohle, R., Romero, I., Schmid, M., Silvester, J.M., Sorella, S., Tocchio, L.F., Wang, L., White, S.R., Wietek, A., Yang, Q., Yang, Y., Zhang, S., Carleo, G.: Variational benchmarks for quantum many-body problems. *Science* **386**(6719), 296–301 (2024) <https://doi.org/10.1126/science.adg9774>
- [31] Zhao, L., Goings, J., Shin, K., Kyoung, W., Fuks, J.I., Kevin Rhee, J.-K., Rhee, Y.M., Wright, K., Nguyen, J., Kim, J., Johri, S.: Orbital-optimized pair-correlated electron simulations on trapped-ion quantum computers. *npj Quantum Information* **9**(1), 60 (2023) <https://doi.org/10.1038/s41534-023-00730-8>
- [32] Robledo-Moreno, J., Motta, M., Haas, H., Javadi-Abhari, A., Jurcevic, P., Kirby, W., Martiel, S., Sharma, K., Sharma, S., Shirakawa, T., Sitdikov, I., Sun, R.-Y., Sung, K.J., Takita, M., Tran, M.C., Yunoki, S., Mezzacapo, A.: Chemistry Beyond Exact Solutions on a Quantum-Centric Supercomputer (2024). <https://arxiv.org/abs/2405.05068>
- [33] Barison, S., Robledo Moreno, J., Motta, M.: Quantum-centric computation of molecular excited states with extended sample-based quantum diagonalization. *Quantum Science and Technology* **10**(2), 025034 (2025) <https://doi.org/10.1088/2058-9565/adb781>
- [34] Trushin, E., Betzinger, M., Blügel, S., Görling, A.: Band gaps, ionization potentials, and electron affinities of periodic electron systems via the adiabatic-connection fluctuation-dissipation theorem. *Phys. Rev. B* **94**, 075123 (2016) <https://doi.org/10.1103/PhysRevB.94.075123>
- [35] Gebauer, R.: Oxygen vacancies in zirconia and their migration: The role of hubbard-u parameters in density functional theory. *Crystals* **13**(4) (2023) <https://doi.org/10.3390/cryst13040574>
- [36] Holmes, A.A., Changlani, H.J., Umrigar, C.J.: Efficient heat-bath sampling in fock space. *Journal of Chemical Theory and Computation* **12**(4), 1561–1571 (2016) <https://doi.org/10.1021/acs.jctc.5b01170>
- [37] Hybertsen, M.S., Louie, S.G.: First-principles theory of quasiparticles: Calculation of band gaps in semiconductors and insulators. *Phys. Rev. Lett.* **55**, 1418–1421 (1985) <https://doi.org/10.1103/PhysRevLett.55.1418>

- [38] French, R.H., Glass, S.J., Ohuchi, F.S., Xu, Y.-N., Ching, W.Y.: Experimental and theoretical determination of the electronic structure and optical properties of three phases of  $\text{zrO}_2$ . *Phys. Rev. B* **49**, 5133–5142 (1994) <https://doi.org/10.1103/PhysRevB.49.5133>
- [39] Králik, B., Chang, E.K., Louie, S.G.: Structural properties and quasiparticle band structure of zirconia. *Phys. Rev. B* **57**, 7027–7036 (1998) <https://doi.org/10.1103/PhysRevB.57.7027>
- [40] Zandiehnam, F., Murray, R.A., Ching, W.Y.: Electronic structures of three phases of zirconium oxide. *Physica B+C* **150**(1), 19–24 (1988) [https://doi.org/10.1016/0378-4363\(88\)90099-X](https://doi.org/10.1016/0378-4363(88)90099-X)
- [41] Dash, L.K., Vast, N., Baranek, P., Cheynet, M.-C., Reining, L.: Electronic structure and electron energy-loss spectroscopy of  $\text{zrO}_2$  zirconia. *Phys. Rev. B* **70**, 245116 (2004) <https://doi.org/10.1103/PhysRevB.70.245116>
- [42] Motta, M., Sung, K.J., Whaley, K.B., Head-Gordon, M., Shee, J.: Bridging physical intuition and hardware efficiency for correlated electronic states: the local unitary cluster jastrow ansatz for electronic structure. *Chem. Sci.* **14**, 11213–11227 (2023) <https://doi.org/10.1039/D3SC02516K>
- [43] Yang, Y.-L., Fan, X.-L., Liu, C., Ran, R.-X.: First principles study of structural and electronic properties of cubic phase of  $\text{zrO}_2$  and  $\text{HfO}_2$ . *Physica B: Condensed Matter* **434**, 7–13 (2014) <https://doi.org/10.1016/j.physb.2013.10.037>
- [44] Jiang, H., Gomez-Abal, R.I., Rinke, P., Scheffler, M.: Electronic band structure of zirconia and hafnia polymorphs from the *gw* perspective. *Phys. Rev. B* **81**, 085119 (2010) <https://doi.org/10.1103/PhysRevB.81.085119>
- [45] Perdew, J.P., Zunger, A.: Self-interaction correction to density-functional approximations for many-electron systems. *Physical Review B* **23**(10), 5048–5079 (1981) <https://doi.org/10.1103/PhysRevB.23.5048>
- [46] Butler, K.T., Frost, J.M., Skelton, J.M., Svane, K.L., Walsh, A.: Computational materials design of crystalline solids. *Chem. Soc. Rev.* **45**, 6138–6146 (2016) <https://doi.org/10.1039/C5CS00841G>
- [47] Giannozzi, P., Baroni, S., Bonini, N., Calandra, M., Car, R., Cavazzoni, C., Ceresoli, D., Chiarotti, G.L., Cococcioni, M., Dabo, I., Dal Corso, A., Gironcoli, S., Fabris, S., Fratesi, G., Gebauer, R., Gerstmann, U., Gougoussis, C., Kokalj, A., Lazzeri, M., Martin-Samos, L., Marzari, N., Mauri, F., Mazzarello, R., Paolini, S., Pasquarello, A., Paulatto, L., Sbraccia, C., Scandolo, S., Sclauzero, G., Seitsonen, A.P., Smogunov, A., Umari, P., Wentzcovitch, R.M.: Quantum espresso: a modular and open-source software project for quantum simulations of materials. *Journal of Physics: Condensed Matter* **21**(39), 395502–19 (2009) <https://doi.org/10.1088/0953-8984/21/39/395502>

- [48] Giannozzi, P., Andreussi, O., Brumme, T., Bunau, O., Nardelli, M.B., Calandra, M., Car, R., Cavazzoni, C., Ceresoli, D., Cococcioni, M., Colonna, N., Carnimeo, I., Corso, A.D., Gironcoli, S., Delugas, P., Jr, R.A.D., Ferretti, A., Floris, A., Fratesi, G., Fugallo, G., Gebauer, R., Gerstmann, U., Giustino, F., Gorni, T., Jia, J., Kawamura, M., Ko, H.-Y., Kokalj, A., Küçükbenli, E., Lazzeri, M., Marsili, M., Marzari, N., Mauri, F., Nguyen, N.L., Nguyen, H.-V., Otero-de-la-Roza, A., Paulatto, L., Poncé, S., Rocca, D., Sabatini, R., Santra, B., Schlipf, M., Seitsonen, A.P., Smogunov, A., Timrov, I., Thonhauser, T., Umari, P., Vast, N., Wu, X., Baroni, S.: Advanced capabilities for materials modelling with quantum espresso. *Journal of Physics: Condensed Matter* **29**(46), 465901 (2017) <https://doi.org/10.1088/1361-648X/aa8f79>
- [49] Giannozzi, P., Baseggio, O., Bonfà, P., Brunato, D., Car, R., Carnimeo, I., Cavazzoni, C., Gironcoli, S., Delugas, P., Ferrari Ruffino, F., Ferretti, A., Marzari, N., Timrov, I., Urru, A., Baroni, S.: Quantum espresso toward the exascale. *The Journal of Chemical Physics* **152**(15), 154105 (2020) <https://doi.org/10.1063/5.0005082> <https://doi.org/10.1063/5.0005082>
- [50] Kittel, C.: *Introduction to Solid State Physics*, 8th edn. John Wiley & Sons, ??? (2004)
- [51] Tantardini, C., Kvashnin, A.G., Ceresoli, D.: Gipaw pseudopotentials of d elements for solid-state nmr. *Materials* **15**(9) (2022) <https://doi.org/10.3390/ma15093347>
- [52] Quantum Espresso pseudopotential data base. <http://www.quantum-espresso.org/pseudopotentials>. Accessed: 2025-03-04
- [53] Ploc, R.A.: The lattice parameter of cubic zro2 formed on zirconium. *Journal of Nuclear Materials* **99**(1), 124–128 (1981) [https://doi.org/10.1016/0022-3115\(81\)90146-X](https://doi.org/10.1016/0022-3115(81)90146-X)
- [54] Prandini, G., Marrazzo, A., Castelli, I.E., Mounet, N., Marzari, N.: Precision and efficiency in solid-state pseudopotential calculations. *npj Computational Materials* **4**(1), 72 (2018) <https://doi.org/10.1038/s41524-018-0127-2> . <http://materialscloud.org/sssp>
- [55] Buongiorno Nardelli, M., Cerasoli, F.T., Costa, M., Curtarolo, S., De Genaro, R., Fornari, M., Liyanage, L., Supka, A.R., Wang, H.: Paoflow: A utility to construct and operate on ab initio hamiltonians from the projections of electronic wavefunctions on atomic orbital bases, including characterization of topological materials. *Computational Materials Science* **143**, 462–472 (2018) <https://doi.org/10.1016/j.commatsci.2017.11.034>
- [56] Cerasoli, F.T., Supka, A.R., Jayaraj, A., Costa, M., Siloi, I., Sławińska, J., Curtarolo, S., Fornari, M., Ceresoli, D., Buongiorno Nardelli, M.: Advanced modeling of materials with paoflow 2.0: New features and software design. *Computational*

- Materials Science **200**, 110828 (2021) <https://doi.org/10.1016/j.commatsci.2021.110828>
- [57] Sun, Q., Berkelbach, T.C., Blunt, N.S., Booth, G.H., Guo, S., Li, Z., Liu, J., McClain, J.D., Sayfutyarova, E.R., Sharma, S., Wouters, S., Chan, G.K.-L.: Pyscf: the python-based simulations of chemistry framework. *WIREs Computational Molecular Science* **8**(1), 1340 (2018) <https://doi.org/10.1002/wcms.1340> <https://wires.onlinelibrary.wiley.com/doi/pdf/10.1002/wcms.1340>
- [58] The ffsim developers: ffsim: Faster Simulations of Fermionic Quantum Circuits. <https://github.com/qiskit-community/ffsim>
- [59] Holmes, A.A., Tubman, N.M., Umrigar, C.J.: Heat-bath configuration interaction: An efficient selected configuration interaction algorithm inspired by heat-bath sampling. *Journal of Chemical Theory and Computation* **12**(8), 3674–3680 (2016) <https://doi.org/10.1021/acs.jctc.6b00407>
- [60] Ezzell, N., Pokharel, B., Tewala, L., Quiroz, G., Lidar, D.A.: Dynamical decoupling for superconducting qubits: A performance survey. *Phys. Rev. Appl.* **20**, 064027 (2023) <https://doi.org/10.1103/PhysRevApplied.20.064027>
- [61] Javadi-Abhari, A., Treinish, M., Krsulich, K., Wood, C.J., Lishman, J., Gacon, J., Martiel, S., Nation, P.D., Bishop, L.S., Cross, A.W., Johnson, B.R., Gambetta, J.M.: Quantum computing with Qiskit (2024). <https://arxiv.org/abs/2405.08810>
- [62] Robertson, N.F., Akhriev, A., Vala, J., Zhuk, S.: Approximate Quantum Compiling for Quantum Simulation: A Tensor Network based approach. *arXiv e-prints* (2023) <https://doi.org/10.48550/arXiv.2301.08609> [arXiv:2301.08609](https://arxiv.org/abs/2301.08609) [quant-ph]
- [63] Garrison, J.R., Marshall, K., Shehzad, I., Sung, K.J., Johnson, C., Rossmannek, M., Fuller, B., Glick, J.R., Akhriev, A., Zhuk, S., Robertson, N.F.: Qiskit Addon: Approximate Quantum Compilation with Tensor Networks. <https://doi.org/10.5281/zenodo.14064353>
- [64] Kállay, M.: Linear-scaling implementation of the direct random-phase approximation. *The Journal of Chemical Physics* **142**(20), 204105 (2015) <https://doi.org/10.1063/1.4921542>
- [65] Niquet, Y.M., Gonze, X.: Band-gap energy in the random-phase approximation to density-functional theory. *Phys. Rev. B* **70**, 245115 (2004) <https://doi.org/10.1103/PhysRevB.70.245115>
- [66] Saki, A.A., Barison, S., Fuller, B., Garrison, J.R., Glick, J.R., Johnson, C., Mezzacapo, A., Robledo-Moreno, J., Rossmannek, M., Schweigert, P., Sitdikov, I., Sung, K.J.: Qiskit Addon: Sample-based Quantum Diagonalization
- [67] Arellano, E., Bello, L., Garrison, J.R., Johnson, C., Robledo-Moreno, J., Sung,

K.J.: Qiskit Addon: Dice Eigensolver